

# The European Russia Drought Atlas (1400–2016 CE)

Edward R. Cook<sup>1</sup> · Olga Solomina<sup>2,3</sup> · Vladimir Matskovsky<sup>2</sup> · Benjamin I. Cook<sup>4</sup> · Leonid Agafonov<sup>5</sup> · Alina Berdnikova<sup>6</sup> · Ekaterina Dolgova<sup>2</sup> · Aleksey Karpukhin<sup>7</sup> · Natallia Knysh<sup>8</sup> · Marina Kulakova<sup>9</sup> · Veronika Kuznetsova<sup>2</sup> · Tomáš Kyncl<sup>10</sup> · Josef Kyncl<sup>10</sup> · Olga Maximova<sup>2</sup> · Irina Panyushkina<sup>11</sup> · Andrea Seim<sup>12</sup> · Denis Tishin<sup>13</sup> · Tomasz Ważny<sup>11,14</sup> · Maxim Yermokhin<sup>8</sup>

Received: 13 July 2019 / Accepted: 31 December 2019 / Published online: 18 January 2020 © Springer-Verlag GmbH Germany, part of Springer Nature 2020

#### **Abstract**

We present the European Russia Drought Atlas (ERDA) that covers the East European Plain to the Ural Mountains from 1400–2016 CE. Like the Old World Drought Atlas (OWDA) for the Euro-Mediterranean region, the ERDA is a one-half degree gridded reconstruction of summer Palmer Drought Severity Indices estimated from a network of annual tree-ring chronologies. Ensemble point-by-point regression is used to generate the ERDA with the identical protocols used for developing the OWDA. Split calibration/validation tests of the ERDA indicate that it has significant skill over most of its domain and is much more skillful than the OWDA where they overlap in the western part of ERDA domain. Comparisons to historical droughts over European Russia additionally support the ERDA's overall validity. The ERDA has been spatially smoothed and infilled using a local regression method to yield a spatially complete drought atlas back to 1400 CE. EOF analysis indicates that there are three principal modes of hydroclimatic variability in the ERDA. After Varimax rotation, these modes correlate significantly with independent climate data sets extending back to the late nineteenth century in a physically interpretable way and relate to atmospheric circulation dynamics of droughts and heatwaves over European Russia based on more recent instrumental data.

 $\textbf{Keywords} \ \ \text{European Russia} \cdot \text{East European plain} \cdot \text{Drought atlas} \cdot \text{Tree-ring network} \cdot \text{Droughts and heat waves}$ 

**Electronic supplementary material** The online version of this article (https://doi.org/10.1007/s00382-019-05115-2) contains supplementary material, which is available to authorized users.

- Lamont-Doherty Earth Observatory of Columbia University, Palisades, NY, USA
- Institute of Geography, Russian Academy of Sciences (RAS), Moscow, Russia
- Faculty of Geography and Geoinformation Technologies, National Research, University Higher School of Economics, Moscow, Russia
- NASA Goddard Institute for Space Studies, New York, NY, USA
- Laboratory of Dendrochronology, Institute of Plant and Animal Ecology, Yekaterinburg, Russia
- Faculty of Geography, Moscow State University, Moscow, Pussia
- Institute of Archaeology, Russian Academy of Sciences (RAS), Moscow, Russia

- <sup>8</sup> Laboratory of Productivity and Stability of Plant Communities, Institute of Experimental Botany, NASB, Minsk, Belarus
- Archaeological Center of Pskovskaya Oblast, Pskov, Russia
- DendroLab Brno, 61600 Brno, Czech Republic
- Laboratory of Tree-Ring Research, University of Arizona, Tucson, USA
- Institute of Forest Sciences, Albert Ludwig University of Freiburg, Freiburg, Germany
- <sup>13</sup> Institute of Environmental Sciences, Kazan Federal University, Kazan, Russia
- Institute for the Study, Restoration and Conservation of Cultural Heritage, Nicolaus Copernicus University, 87-100 Torun, Poland



#### 1 Introduction

For many centuries, the Russian economy was fully dependent on the cereal harvests of important grain crops such as wheat, rye, and barley. Before the development of the virgin and highly fertile Black Earth or Chernozem soils for farming in Kazakhstan and southern Siberia in the twentieth century, Russian agriculture was mainly concentrated in the European territories west of the Ural Mountains where most of the population was living. However, because of its high latitude location and continentality, European Russia (that part of Russia extending from its westernmost political border eastward to the Urals) was always a land of "risky agriculture" where harvest yields were often below expectation due to adverse weather conditions (Golubev and Dronin 2004; Dronin and Bellinger 2005). Crops in the more northerly lands often suffered from cold and wet summers, late frosts in the spring, and early frosts in the autumn, while the southern and eastern "bread basket" territories of European Russia were regularly affected by severe droughts in the summer. Many of the current "bread basket" areas of Russia, including the Chernozem lands, the lower Volga region, and the southern part of Siberia, are projected to experience reductions in rain-fed spring wheat yields before the end of the twenty-first century under multiple climate change scenarios due to an increase in aridity driven primarily by a projected decrease in precipitation (Pavlova et al. 2019). Similar reduced grain yield projections can be found in Kiselev et al. (2013) for rain-fed crops.

Climate perturbations have always strongly affected the Russian economy and social life, as far back as medieval times (Klimenko and Solomina 2010). Droughts leading to poor crops provoked social instability and sometimes large-scale riots and revolts. Historical chronicles from monasteries starting in the beginning of the past millennium provide direct information on local and regional droughts, but they also mention "hungers", increases of grain prices, and other social phenomena indirectly connected to impacts of climatic extremes. Unfortunately, these historical records are heterogeneous in time (availability decreases back in time) and in space (records mainly from regions where monasteries are located).

Borisenkov and Pasetsky (1988) indicate that the number of recorded droughts increased from 18 in the tenth century to 70 in the nineteenth century. Conversely, the number of rainy summers increased from 6 to 53, and the number of famines from 13 to 85, over the same time period. It is not clear how much of these trends are connected to uneven historical information or are reflections of changing climatic conditions. To determine so requires an independent source of past hydroclimatic variability

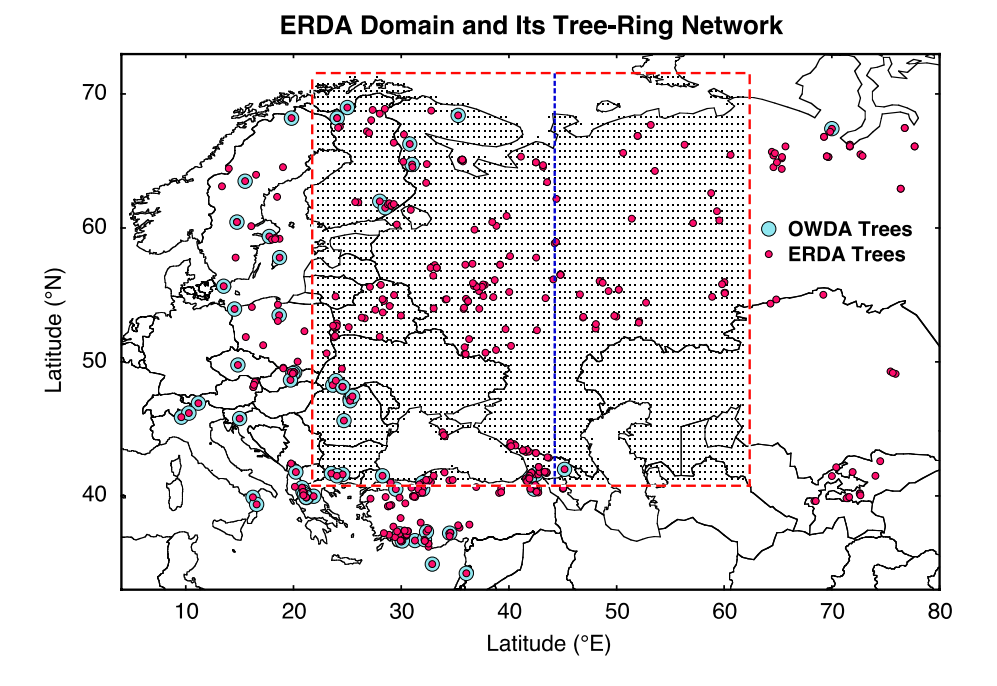
over European Russia extending back hundreds of years in the past, hence the need for a high-quality tree-ring drought atlas that is specifically targeted to this region.

The existing Old World Drought Atlas (OWDA) (Cook et al. 2015) covering the Euro-Mediterranean region appears to fill much of this information gap. However, it is not adequate for assessing past droughts over European Russia for two reasons. First, the eastern limit of the OWDA domain only extends half way across the East European (Russian) Plain and therefore does not fully cover the grain producing areas there. Second, the tree-ring network used to produce the OWDA included only ten tree-ring chronologies from within the former European USSR sector: four from northwest Russia, four from western Ukraine, and two from Georgia. The drought reconstructions from the Russian region of the OWDA are consequently weak with low model validation skill (see Fig. S11 in the Supplementary Materials of Cook et al. 2015 and below). These limitations render the OWDA inadequate for investigating past periods of unusual drought and wetness in European Russia.

The frequency and severity of droughts in European Russia has been studied since the mid-twentieth century using hydrometeorological records (Rudenko 1958; Drozdov 1980; Meshcherskaya and Blazhevich 1997; Cherenkova 2007; Schubert et al. 2014), historical data (Bogolepov 1907, 1922; Buchinsky 1957; Borisenkov and Pasetsky 1988, 2003; Voronov 1992), stratigraphy of lake sediments (Shostakovich 1934; Rauner 1981), and tree-rings (Shvedov 1892; Chernavskaya 1995; Krenke and Chernavskaya 1998; Matveev et al. 2012a, b; Solomina et al. 2005, 2012, 2017; Matskovsky et al. 2017). Successful reconstructions of drought from tree rings in southern Finland across the border from Russia are also noteworthy (Helama and Lindholm 2003; Seftigen et al. 2015, 2017). However, high-resolution and spatially complete field reconstructions of past drought and wetness for the full European Russia area have been unavailable. To fill this information gap, we have developed and present herein the European Russia Drought Atlas (ERDA) covering the period 1400–2016 CE. The ERDA is a 4259-point field reconstruction of the June-July-August (JJA) average self-calibrating Palmer Drought Severity Index (scPDSI) (Wells et al. 2004; van der Schrier et al. 2013) based on a greatly improved network of 697 annual tree-ring chronologies distributed over the ERDA domain (Fig. 1). In addition, this domain now includes all of European Russia, providing a high-quality spatiotemporal reconstruction that we can use to analyze summer season drought variability in the region over the last ~600 years.



Fig. 1 Map of the European Russia Drought Atlas (ERDA) domain circumscribed by the red dashed rectangle: 4259 one-half degree grid points of JJA scPDSI. The network of tree-ring chronologies used in the ERDA are shown by small red dots and those used in the OWDA as large blue dots. The vertical blue dashed line is the western limit of the old world drought atlas, which illustrates the inadequate spatial coverage of that domain over European Russia



## 2 Regional climate setting

The East European Plain is located in the high-to-mid latitudes between the Arctic Ocean to the north, the Black and Caspian Seas to the south, and from the Polish/Ukraine frontier in the west to the western slope of the Urals Mountains in the east (Fig. 1). The radiation balance in winter is negative for the whole East European Plain except for the southernmost territories, while in summer it is positive everywhere. The climate is most strongly influenced by the westerlies. Air masses from the Atlantic Ocean in winter bring warmth and precipitation, while in summer they are responsible for cool and wet weather conditions. Because of increased continentality, air masses are drier as one moves east and are also warmer in summer and colder in winter (Klimenko and Solomina 2010).

Summer season droughts and heat waves over this region are typically caused by persistent anticyclones (Obukhov et al. 1984; Schubert et al. 2014; Stefanon et al. 2012), often originating from the Arctic (Buchinsky 1976; Kleschenko 2005) and associated with quasi-stationary Rossby wave trains (Schubert et al. 2011, 2014). Dry and hot conditions in European Russia are often concurrent with cool and wet conditions to the east or west, further highlighting the importance of zonal wave structures in the atmosphere for summer season climate variability in the region (Gershunov and Douville 2008). A canonical example of such a pattern was observed in the summer of 2010, when a stationary Rossby wave simultaneously caused the occurrence of extreme drought and heat in European Russia and severe precipitation and flooding in Pakistan (Lau and Kim 2012; Schubert et al. 2011). These summer circulation anomalies over European Russia arise predominately from internal atmospheric variability (Schubert et al. 2014, 2016), and may be associated with the Eastern Atlantic/Western Russia (EA/WR) and Scandinavian (SCA) patterns (Rocheva 2012).

Alisov (1969) subdivides the territory of the East European Plain into three climatic areas: 1. Northern Atlantic-Arctic area (southern boundary located between Lake Ladoga near St. Petersburg and the Pechora River in northwest Russia). 2. Middle Atlantic-continental area (southern boundary from the mid-Dniester to the mid-Volga Rivers). 3. Southern continental area. The areas are also subdivided into the western and eastern sub-areas with the boundary running from the Northern Dvina River to the mouth of the Dnieper River. The climate is mirrored by the vegetation and soil zones. The major zones contained within the East European Plain from north to south are tundra, forest-tundra, forest-steppe, semi-desert and desert.

The longest instrumental records in Eastern Europe go back to the mid-eighteenth century. Gazina and Klimenko (2008) analyzed winter, summer, and annual temperature variations of the four longest meteorological stations in Eastern Europe that have few or no gaps (St. Petersburg, Vilnius, Moscow, and Riga). For this analysis, they used the data in the databank RIHMI-WDC (http://www.meteo.ru/data/mdata.htm) as well as earlier records of Kupfer (1846), Veselovsky (1857), Vil'd (1882), and Wahlén (1886). Gazina and Klimenko (2008) found that during the last two centuries winter temperatures have increased (up to 3 °C) at all four stations, while summer temperatures have decreased. These findings contrast with Western Europe, where both winter and summer warming have occurred. In general, precipitation is also much more variable than temperature between



regions across the East European Plain. Annual precipitation amounts in northern (St. Petersburg) and central (Moscow) parts of the Plain are highly correlated. This is also the case for southern (Kiev and Odessa) parts of the Plain. However, differences in inter-annual variability and long-term trend in annual precipitation between the north and south are quite large. The increase in annual precipitation over the last 150 years is significant both in Moscow and St. Petersburg, but the trend is insignificant in the southern regions.

#### 3 Data

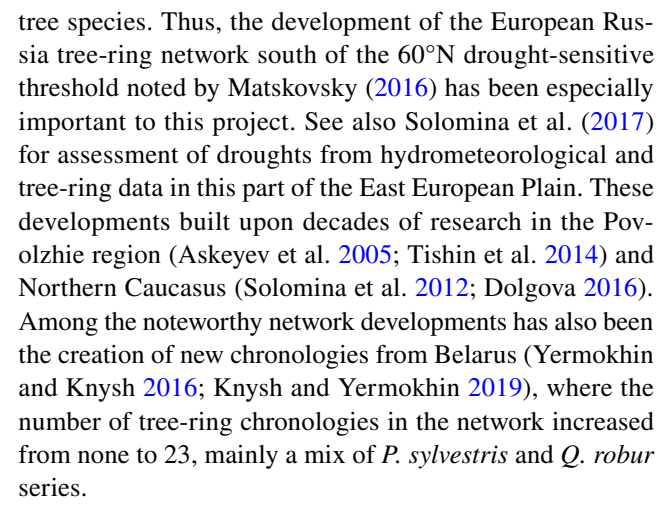
#### 3.1 Climate data sets

The scPDSI data used here as the target field for reconstruction is based on CRU TS 3.25 gridded temperature and precipitation data (Osborn et al. 2017; 0.5° resolution). It covers the period 1901–2016. See https://crudata.uea.ac.uk/cru/data/drought/ for details. Other climate data sets used here for analyses of the ERDA include Global Precipitation Climatology Centre precipitation (GPCC; Schneider et al. 2018; 1.0° resolution), Berkeley Earth global temperature (BEST; Muller et al. 2013; 1.0° resolution), UCAR global scPDSI (UCAR; Dai and Zhao 2017; 2.5° resolution), and upper air data from the twentieth Century Reanalysis (Compo et al. 2011; 2.0° resolution). These latter data sets are available for use at KNMI Climate Explorer (van Oldenborgh and Burgers 2005; Trouet and van Oldenborgh 2013; http://climexp.knmi.nl/).

#### 3.2 Tree-ring data

Figure 1 shows the distribution of tree-ring chronologies used in developing the ERDA, a total of 697 chronologies in all, many of them developed specifically for this project. Within just European Russia itself, the network has increased from only four chronologies used in the OWDA to 275 chronologies used here. This includes tree-ring series from eight species: *Pinus sylvestris* L. (156 series), *Larix sibirica* Ledeb. (39 series), *Picea obovata* Ledeb. (33 series), *Picea abies* (L.) H. Karst. (32 series), *Quercus robur* L. (9 series), *Abies nordmanniana* (Stev.) Spach (3 series), *Fagus orientalis* Lipsky (2 series), and *Pinus halepensis* Mill. (1 series).

Recently, strong efforts have been made to sample in areas south of the taiga regions in the hotter and more droughty parts of European Russia where the tree-ring network has been historically very sparse. Matskovsky (2016) analyzed the climate sensitivity of ring widths for the most common species growing on the overall East European Plain and concluded that the region located at 55–60°N is the approximate border between temperature and drought sensitive conifer



In addition to the chronologies lying inside the ERDA domain, chronologies surrounding this area are included to the dataset (Fig. 1). They are chronologies from Eastern and Central Europe (Cook et al. 2015), from Western Siberia (Agafonov and Gurskaya 2012, 2013; Gurskaya et al. 2012; Agafonov et al. 2016), and the Central Asia countries of Kyrgyzstan (Graybill et al. 1992; Esper et al. 2003; Solomina et al. 2012, 2014; Seim et al. 2016a), Kazakhstan (L. Agafonov, A. Berdnokova, unpubl. data), and Uzbekistan (Seim et al. 2016b).

European Russia is also an area where ancient populations traditionally used wood for construction, heating, and other purposes. The original old-growth forests were also cleared for agriculture. These activities, along with climate contributing to the rapid decay of wood, are the reasons why old wood collections are quite rare in the region. After the archaeological Novgorod chronology (Kolchin 1963) was constructed, only a few composite chronologies based on archeological, historical, and modern (living) wood samples covering a substantial part of the past millennium have been constructed (Solomina et al. 2011, 2017; Karpukhin and Matskovsky 2014; Tarabardina 2009; Kulakova 2009). This limits the useful length to the ERDA to 1400–2016 CE at present.

## 3.3 Tree-ring network suitability

The suitability of the ERDA tree-ring network for drought reconstruction brings into consideration the issue of whether or not some boreal forest tree-ring series can be used for reconstructing drought there. At the more southerly warmer and drier sites, we expect tree radial growth to be frequently limited by soil moisture availability (Matskovsky 2016; Solomina et al. 2017), thus resulting in a positive correlation between tree rings and scPDSI there. However, as site locations approach the cooler northern tree line limit, we expect radial growth to become more frequently limited by growing season temperature (Hellmann et al. 2016). This



change in tree growth response to climate can result in a negative correlation between tree rings and scPDSI through a clear sky-evapotranspiration demand signal, which is not directly related to precipitation and soil moisture content, but is still correlates with site hydroclimatic conditions. Regardless, this is not optimal because the variability in ring width induced by evapotranspiration demand in temperature-sensitive trees may differ in meaningful ways from that induced by soil moisture availability in moisture-sensitive trees. We therefore accept that using temperature-sensitive tree-ring series for drought reconstruction may be problematic if used in isolation, e.g. only from the Polar Urals (Briffa et al. 1995). However, the inverse relationship driven by evapotranspiration demand is not universal even in the high northern latitudes because temperature sensitivity there varies considerably in strength due to varying site locations and conditions (St George and Ault 2014; Hellmann et al. 2016). Thus, Hellmann et al. (2016) reported that north of 60°N (cf. Matskovsky 2016) only 16.6% of Eurasian boreal forest tree-rings chronologies had statistically significant positive correlations with June-July average temperature (mostly at higher latitude sites  $> 65^{\circ}$ N), and they also found a number of tree-ring chronologies to be positively correlated (r>0.30) with June-July precipitation there as well (their Fig. 4d). Similar results for Fennoscandia are also described in Babst et al. (2013). Given that each grid point of scPDSI being reconstructed in the ERDA is based on a minimum of 20 tree-ring series located within either 500 or 1000 km of the grid point (see below in Sect. 4), with a variable range of both positive and negative correlations with scPDSI, we do not consider the use of negatively correlated tree-ring predictors of scPDSI to be a problem here.

#### 4 Methods

## 4.1 Tree-ring standardization

The 697 tree-ring chronologies used for reconstruction were standardized (sensu Fritts 1976) in a relatively uniform way using state-of-the-art tree-ring standardization methods based on 'signal free' detrending (Melvin and Briffa 2008) to eliminate trend-distortion artefacts and maximally preserve common medium frequency variance among series. In addition, we used the age-dependent spline (Melvin et al. 2007) to conservatively remove low-frequency variance thought to be mainly due to non-climatic age/size-related changes in ring width over time. This combination minimizes the loss of common variance due to the 'segment length curse' (Cook et al. 1995). In addition, adaptive power transformations were applied to the raw ring-width measurements prior to detrending to render them more homoscedastic. Doing so enabled the tree-ring indices to be calculated as residuals

rather than ratios to reduce the likelihood of index calculation bias in the estimation of the tree-ring chronologies (Cook and Peters 1997).

## 4.2 Ensemble point-by-point regression

Ensemble point-by-point regression (EPPR) was used to produce the ERDA. It is a generalization of the original PPR method (Cook et al. 1999) whereby each tree-ring chronology found within a given search radius around each grid point is weighted by some power of its correlation with the climate variable being reconstructed. See Cook et al. (2013, 2015) and the Supplementary Materials for details. The correlation-weighted chronologies are then used in the principal components regression (PCR) model at each grid point for reconstructing climate from tree rings. This is done in lieu of selecting a subset of chronologies based on a fixed correlation screening probability. For the ERDA we used two tree-ring search radii, 500 and 1000 km, for locating the tree-ring chronologies for reconstructing each scPDSI grid point, with a minimum of 20 chronologies used for each grid point reconstruction. This resulted in a 16-member ensemble (eight per search radius), which was then robustly averaged for further use.

The EPPR method used here is identical to that used in creating the OWDA (Cook et al. 2015), which makes a one-to-one comparison of calibration and validation skill between the two drought atlases possible for the common region of overlap indicated in Fig. 1. This comparison will be shown later.

#### 4.3 Queen's case imputation and smoothing

Here we introduce Queen's case imputation and smoothing (QCIS) and describe why it was developed. EPPR produces reconstruction fields that are spatially complete as far back as the first year of the shortest grid point reconstruction produced. Earlier than that, spatial gaps in the annual reconstructed fields develop, and these gaps increase in size back in time because some grid point reconstructions are longer than others due to the varying tree-ring chronology lengths used. In addition, there can be "checker board" patterns in the reconstructed fields produced in part by random effects in the EPPR procedure at the grid point level. These properties imply the need to both locally impute and smooth the ERDA fields in a way that is consistent with the pointwise regression design of EPPR.

To this end, we developed a nine-point regression kernel method called Queen's Case Imputation and Smoothing (QCIS) and applied it to each grid point reconstruction produced by EPPR to re-estimate, locally smooth, and infill spatial gaps in the fields back to 1400 CE. For consistency with the original EPPR results, QCIS uses the same PCR



method as EPPR, the same grid point instrumental data for recalibration, and reports the same calibration/validation period statistics. Thus, QCIS is designed to produce a locally smoothed and infilled field reconstruction that is consistent with the original pointwise design of PPR (Cook et al. 1999). The smoothing effects of QCIS on the reconstructions in both space and time is described in the Supplementary Materials. It is shown there that QCIS predictably smooths the spatial patterns, but has little effect on the temporal variability of the grid point reconstructions at the spatial scale investigated here.

#### 4.4 Calibration and validation

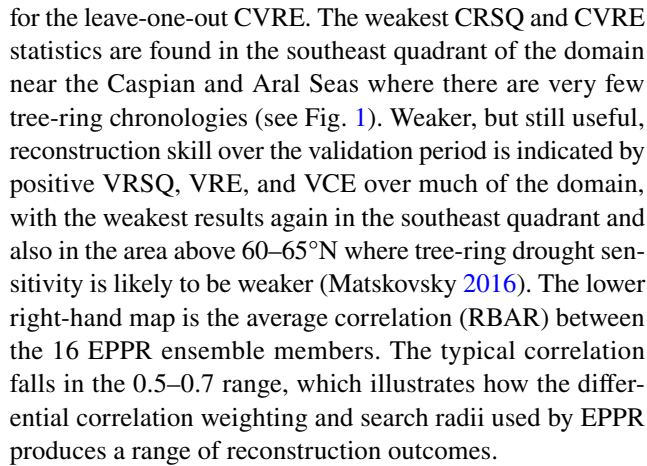
The instrumental scPDSI data used for statistical calibration and validation cover the 1901–2016 period. In contrast, the tree-ring chronologies have a common end year of 1983 because of the widely varying years in which the trees were sampled. For this reason, the calibration period chosen for developing the reconstructions was 1931–1983. The remaining 1901–1930 scPDSI data were withheld from the calibration exercise for use in model validation testing (Berk 1984; Picard and Berk 1990). This style of split calibration/validation testing is described in Fritts (1976) and has been used successfully in the development of all previous drought atlases beginning with Cook et al. (1999).

The calibration period statistics reported here are the coefficient of determination (R<sup>2</sup> or CRSQ) and a leave-one-out cross-validation statistic (CVRE). CVRE is the R<sup>2</sup> version of the Prediction Error Sum of Squares (PRESS) statistic (Allen 1974; Quan 1988) and, thus, provides a less biased expression of explained variance compared to CRSQ. In poorly calibrated cases, CVRE can actually be negative, which is impossible for CRSQ.

The validation statistics reported here are the square of the Pearson correlation (VRSQ), the reduction of error (VRE), and the coefficient of efficiency (VCE). When VRSQ, VRE, and VCE are positive, they are different measures of model skill expressed in units of fractional explained variance over the validation period. Negative values indicate no reconstruction skill as measured. In addition, the formulae of these statistics require that VRSQ≥VRE≥ VCE when calculated from the same data, thus making VCE the hardest validation statistic to pass. See Cook et al. (1994, 1999) for detailed descriptions of these model validation statistics.

## 5 Calibration and validation results

The ERDA calibration and validation maps based on the EPPR 16-member ensemble mean field are shown in Fig. 2. Overall, the calibration period CRSQ exceeds 40% of the total scPDSI variance at most grid points. The same is true



The calibration and validation results presented in Fig. 2 strongly support the overall validity of the ERDA. Nonetheless, it is useful to show the degree to which they are better than those of the OWDA in the overlapping domain regions shown in Fig. 1. Figure 3 compares the ERDA and OWDA using two calibration statistics (CRSQ and CVRE) and one validation statistic (VRSQ). This comparison shows that the ERDA is far more skillful than the OWDA over most of their shared domains. An exception is in southern Finland, where both the OWDA and ERDA calibrate and validate well as expected based on past drought reconstruction success there by Helama and Lindholm (2003) and Seftigen et al. (2015, 2017). Since the scPDSI data and EPPR methods used are the same for each drought atlas, the only plausible explanation for the improved calibration/validation skill over the ERDA domain is its vastly improved tree-ring network used for reconstruction.

## 6 Rotated EOF analysis

The ERDA is made up of 4259 grid points of one-half degree scPDSI covering the common period 1400–2016. As described earlier, complete spatial coverage back to 1400 was achieved by applying QCIS to the original ensemble member fields before averaging. In the process, QCIS locally smoothed the fields to reduce "checker board" patterns. See the Supplementary Materials for details. QCIS was applied to all data up to 2016, but only the data up to 1983 are based on tree-ring estimates. It is the tree-ring-only portion of the ERDA from 1400 to 1983 that will be evaluated now using empirical orthogonal function (EOF) analysis.

EOF analysis has a long history of use in climatological studies (e.g. Lorenz 1956; Kutzbach 1967) and in tree-ring analyses (e.g. LaMarche and Fritts 1971; Fritts 1976) because it distills the complex variability contained in a sequence of climate and tree-ring fields into a greatly reduced subset of orthogonal fields for potentially easier interpretation and application. However, as pointed out by



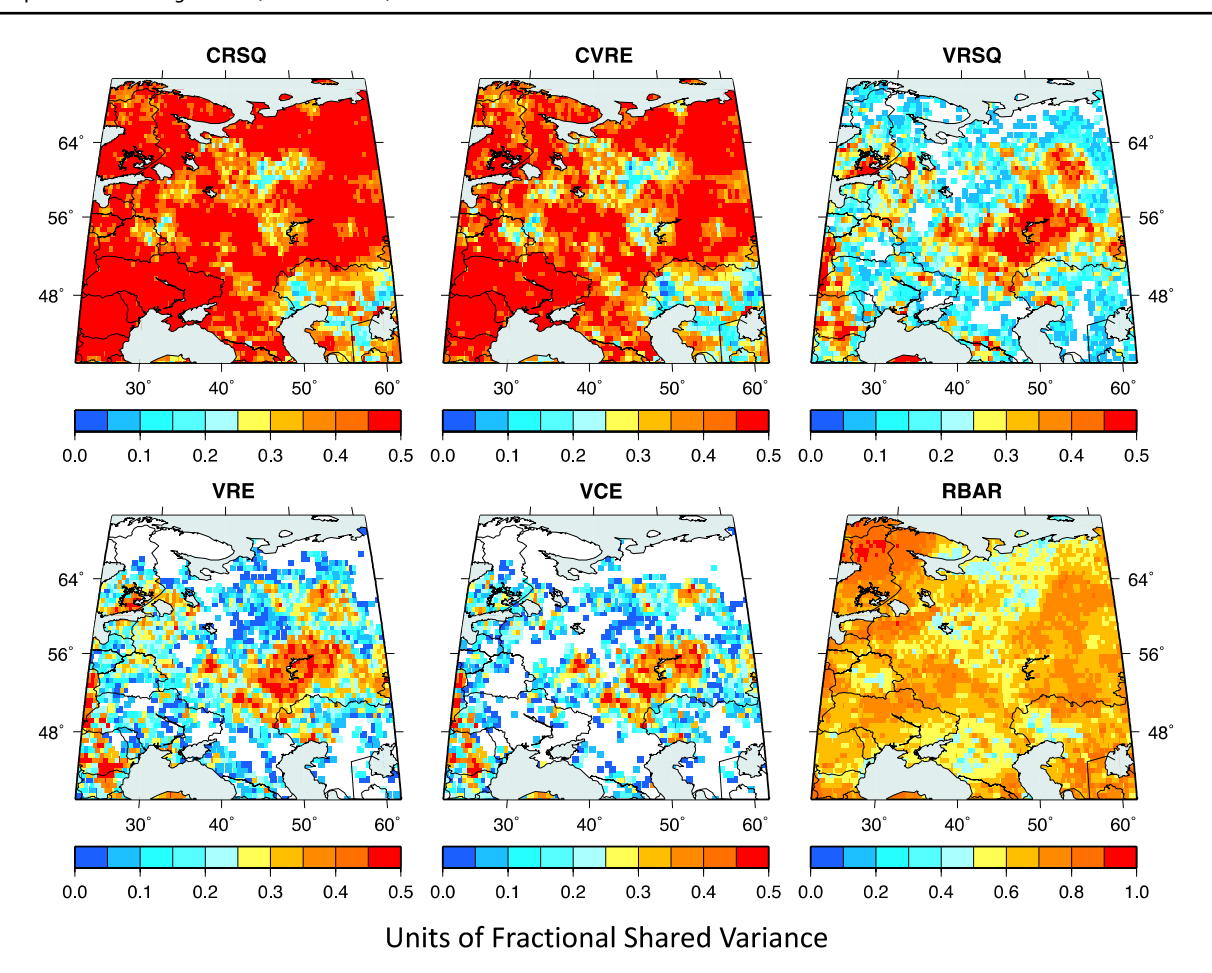


**Fig. 2** Calibration and validation maps for the ERDA based on an ensemble average of 16 PPR runs as described. *CRSQ* calibration period R<sup>2</sup>, *CVRE* calibration period leave-one-out cross-validation, *VRSQ* validation period square of the Pearson correlation, *VRE* vali-

dation period reduction of error, *VCE* validation period coefficient of efficiency, *RBAR* average correlation (RBAR) between the 16 ensemble members

Richman (1986), care must be applied in interpreting EOFs as realistic expressions of natural climate variability because of the mathematical constraints applied to their estimation.

A common way to reduce the well known limitations of EOFs for physical interpretation is to apply analytical rotation to a subset of EOFs. There are many ways to do this (Richman 1986), but we chose here the widely used normalized Varimax method (Kaiser 1958). This rotation method has been used with considerable success in characterizing the space—time patterns variability of climate fields, such as those related to the quasi-stationary modes of upper-air atmospheric circulation (Barnston and Livezey 1987) and to fields of PDSI based on both instrumental (Karl and Koscielny 1982) and reconstructed (Cook et al. 1999) data.

The application of Varimax rotation requires a reasonably well estimated subset of EOFs (the "signal subspace") to rotate. There are many ways this might be determined (Preisendorfer et al. 1981), but it is complicated by the rank deficiency of the ERDA correlation matrix, which is based on 4259 (m) grid points and 584 (n) years of data. For centered

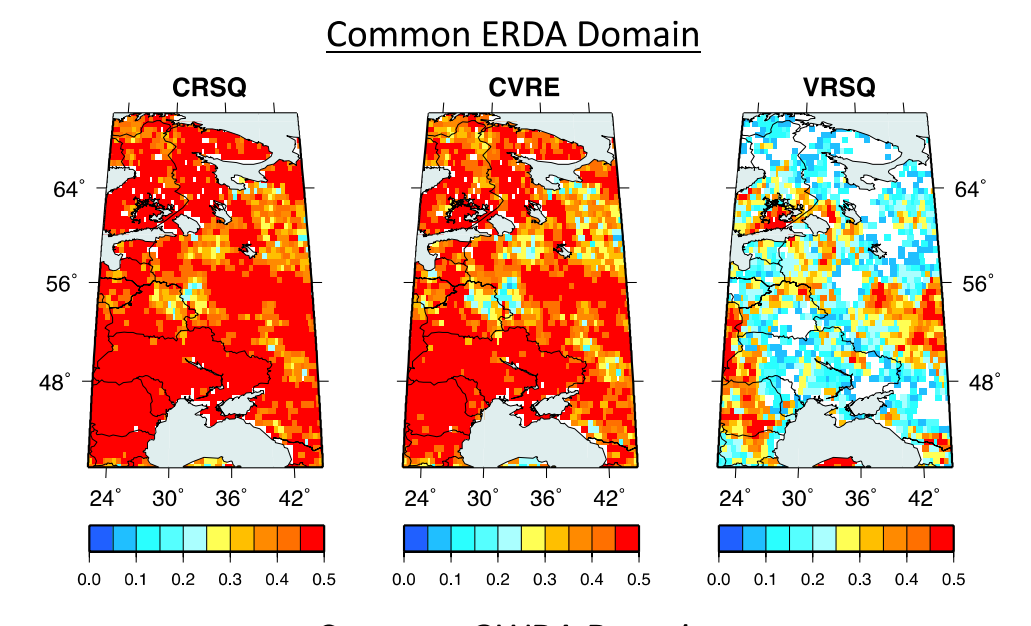
data, the total number of defined EOFs is min(n-1,m), or only 583 in the case of the ERDA. This renders asymptotic methods such as the Kaiser-Guttman eigenvalue-1 cutoff rule (Guttman 1954; Kaiser 1960) quite useless to apply. It also degrades the performance of monte-carlo methods like the 'Rule N' method (Preisendorfer et al. 1981). Therefore, we have chosen a very simple method based on the visual "scree test" of the eigenvalue trace (Cattell 1966), with the added application of the "North test" for separation of eigenvalues (North et al. 1982).

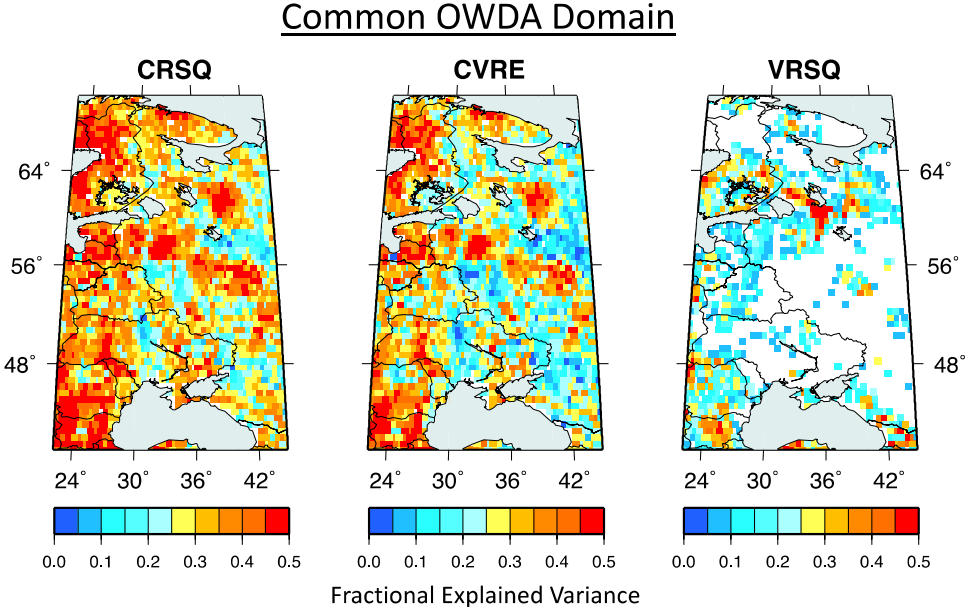
Figure 4 shows the eigenvalue trace out to order-10 calculated from the ERDA correlation matrix. There is no point in showing more because the cumulative variance trace shows that the first ten eigenvalues already account for 73.9% of the total variance. Each eigenvalue has its uncertainty expressed as  $\pm 2$  standard errors as estimated by the equation provided by North et al. (1982). The first three eigenvalues separate cleanly from the rest, even after considering their 2-standard error uncertainties, and account for 42.5% of total variance. This indicates that there are only three EOFs in the signal



Fig. 3 Comparisons of calibration/validation statistics in the domain area common to the ERDA and OWDA. See Fig. 1 for the location of that area to the left (west) of the dashed vertical blue line. Two calibration (CRSQ and CVRE) and one validation (VRSQ) for each are shown. The differences in both calibration and validation are very clear. The ERDA has clearly better skill due to its vastly improved tree-ring network

# Comparisons of Calibration/Validation Results Common to the ERDA and OWDA Domains





subspace worth rotating. The sharp break in the eigenvalue trace after the third eigenvalue may reflect in part the application of QCIS to the ERDA because QCIS will emphasize larger-scale patterns due to its spatial smoothing effect (e.g. Fig. SM4) and thus lose some local details related to reconstructed wet and dry anomalies that occupy only a small part of the domain. This was considered an acceptable cost in order to infill the ERDA completely back to 1400 CE.

The EOFs before and after rotation (the Varimax factors or VFs) are shown in Fig. 5 for comparison, along with the variance accounted for by each. There is relatively little

difference between them, and the total variance (42.5%) after rotation is exactly conserved as required by the Varimax method. However, the regional expressions of drought and wetness are more cleanly separated after rotation. They represent three principal areas of the ERDA domain: interior European Russia east of ~40°E (VF1), northwestern Russia, Finland and the Baltic States (VF2), and southwestern Russia, Belarus, Ukraine, Moldova, and Romania (VF3). The area most weakly represented by any of these factors is in the southeastern quadrant where calibration was relatively weak (Fig. 2) and the effect of QCIS was the greatest (Fig. SM4).



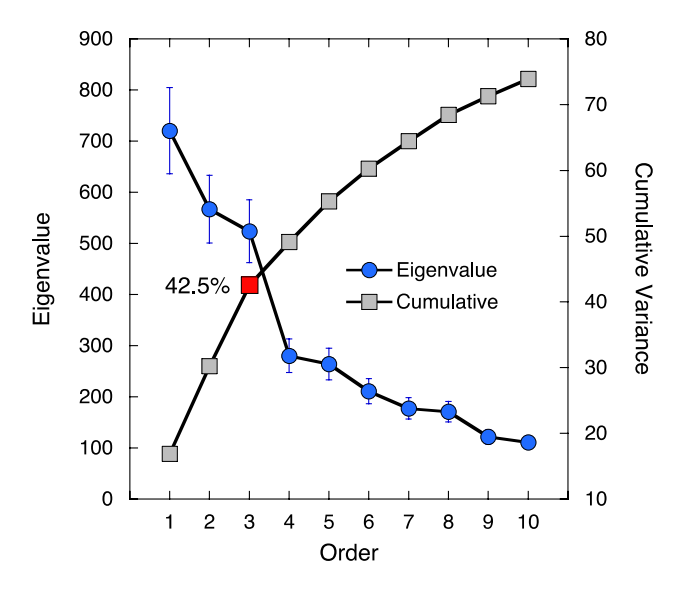


Fig. 4 The eigenvalue trace of the ERDA (1400-1983) plotted out to order 10, and the cumulative variance accounted for by those first 10 unrotated EOFs. The uncertainties in the eigenvalues are expressed as  $\pm 2$  standard errors (vertical bars) based on the standard error estimate from North et al. (1982). The first three eigenvalues separate cleanly from the rest and account for 42.5% of total variance, thus determining the eigenvalue cutoff (red square) for Varimax rotation

Figure 6 shows plots of the VF scores (Fig. 6a–c) corresponding to their respective factor patterns shown in Fig. 5. In addition, the mean of the three factor scores (Fig. 6d) is intended to highlight occurrences of 'pan-ERDA' dry and wet years. Since the Varimax factor scores are orthogonal, the mean should preserve the occasional years when these events co-occur and at the same time dampen out other variability not common to the three factors.

Each series in Fig. 6 has been expressed in terms of standard deviations from the mean, with a ten-year low-pass filter (red) applied to each to emphasize mult-year variability in drought and wetness. The horizontal dashed lines are the  $\pm 2$  standard deviation limits used for identifying years of severe drought and wetness. Notable years of severe drought are 1936, 1841, 1757 for VF1, 1408, 1940, 1826 for VF2, and 1453, 1921, 1939 for VF3. The top three drought years in the mean 'pan-ERDA' series are 1939, 1921, and 1659. A complete list of dry and wet years exceeding  $\pm 2$  standard deviation limits in Fig. 6 is provided in Table 1. Overall, there is a somewhat higher frequency of extreme drought years indicated since 1800, with 1921 and the 1930s standing out in particular. In contrast, unusually wet years appear to be more evenly distributed over time.

Care must be taken, however, in interpreting Table 1 as a comprehensive list of ERDA extremes because it does not contain some of the more important wet and dry years in the ERDA. The ones identified in Fig. 6 primarily reflect those years with spatial patterns of reconstructed scPDSI

that are reasonably close to their respective Varimax factor patterns in Fig. 5. Thus, some known severe droughts over parts of the ERDA domain that do not match the Fig. 5 patterns expecially well are not evident in the Table 1 list. For example, the severe 1946 drought in Ukraine and Moldova (Volkov 1992; Potop and Soukup 2009) is strongly evident in the ERDA (not shown), but is not in the list because the overall spatial pattern of reconstructed scPDSI over the entire ERDA domain for that year does not strongly match the Varimax factor #3. Other methods of identifying wet and dry year extremes in the ERDA, e.g. by calculating drought area indices (Mitchell et al. 1979; Bhalme and Mooley 1980), might be more appropriate depending on the goals of the analysis. Here we are primarily interested in objectively identifying the principal large-scale modes of variability in the ERDA through REOF analysis and how they are related to atmospheric circulation (see Sect. 8).

Using the factor scores plotted in Fig. 6a–c, additional validation testing was conducted on the ERDA. This was done using GPCC precipitation, BEST temperature, and UCAR scPDSI gridded data (refer to "Climate data sets" above) for the same JJA season as the ERDA reconstruction. The 1891–1930 pre-calibration period was used for these "out-of-sample" tests of the ERDA factor scores based now on ten additional years of data over that used previously for validation.

Figure 7 shows correlation maps for Varimax factors VF1-VF3 versus GPCC, BEST, and UCAR climate data. Correlations > 10.41 are significant at the 99% confidence level. The rectangle shown in each map delineates the boundaries of the ERDA. After comparing the GPCC, BEST, and UCAR correlation patterns with the Varimax factor patterns (Fig. 5), the highest climate correlations can be seen to largely fall in the same locations as the highest factor loadings, a result that supports the climate interpretations of these empirical modes. In particular, the temperature correlation pattern in VF1 is similar to the East Atlantic/ Western Russia (EA/WR) pattern for summer (Barnston and Livezey 1987; their Eurasia-2 pattern), with the main center of action north of the Black and Caspian Seas. The strongest monthly correlation between the EA/WR index and VF1 is for May (r = 0.45, p < 0.01) for the 1950–1983 period. There is also some similarity between VF2 and the Scandinavian (SCAND) pattern (Barnston and Livezey 1987; their Eurasia-1 pattern), characterized by a meridional dipole in both temperature and precipitation with a strong locus over Scandinavia. In this case the strongest correlation between SCAND and VF2 is for the month of March (r = -0.48,p < 0.01).

Schubert et al. (2014) applied rotated EOF (REOF) analysis to the joint summer (JJA) temperature and precipitation fields over northern Eurasia, which fully includes the ERDA domain. Their REOF1 temperature and precipitation factor



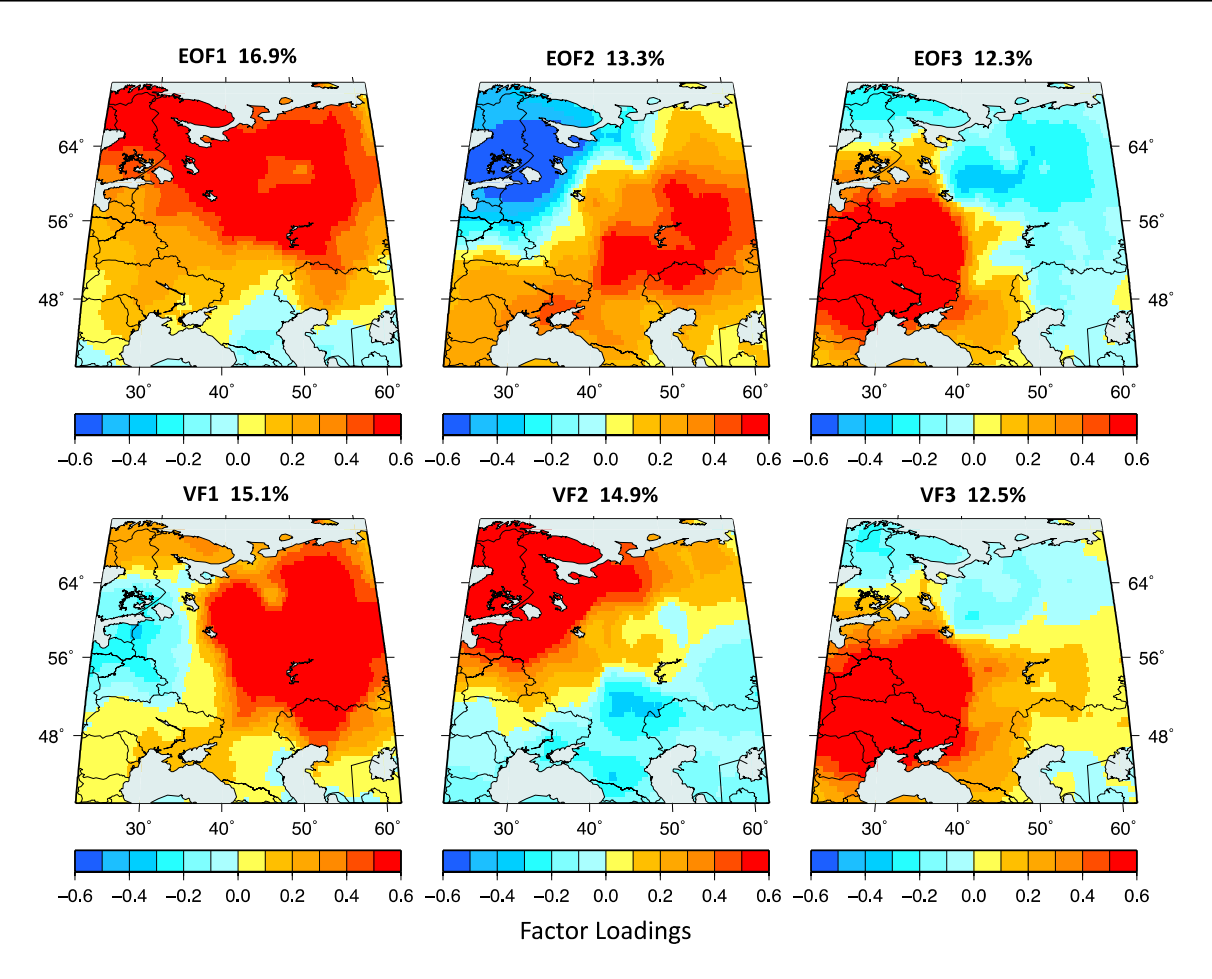


Fig. 5 The first three unrotated (EOF) and Varimax rotated (VF) factors, with the variance accounted for by each factor indicated. There is little difference in the variance accounted for before and after rotations.

tion, and the total variance (42.5%) is exactly conserved after rotation, but the regional expressions of drought are more cleanly separated after Varimax rotation

patterns (fig. 3 in Schubert et al. 2014) include high loadings over the ERDA VF1 region. Similar spatial congruence can also be found between their REOF5 factor patterns and that shown here in VF3. Given the relatively short analysis period (1979–2012) used by Schubert et al. (2014), plus their much larger analysis domain, this level of agreement suggests a robust link between the hydroclimatic variability expressed in the ERDA and much larger scale atmospheric circulation features across all of northern Eurasia.

Figure 8 shows composites of the notable dry and wet years indicated in Fig. 6 and listed in Table 1. For the most part the dry and wet composites are near-mirror images of each other, suggesting a linear association between the occurrence of these extreme patterns and their causal mechanisms. The clear exception is the asymmetry in the patterns associated with VF3 over western Russia, Belarus, and Ukraine. The dry year pattern extends zonally across most of European Russia, with a small pattern of wetness north of about 62°N. In contrast, the VF3 wet year pattern exhibits a strongly meridional west-to-east change from wet to dry.

The ERDA factor scores do not reveal the occurrence of severe long-duration droughts (i.e. megadroughts) over European Russia and surrounding countries like those found in the American West (Cook et al. 2004). This is consistent with the understanding that individual drought events across European Russia rarely exceed 50 days in duration (Cherenkova 2007; Schubert et al. 2014). The longest period of mostly below-average scPDSI in the ERDA factor scores occurred over a 26-year period from 1784 to 1809. Few individual drought years stand out during this time, but the overall cumulative moisture deficit would have been large. This period of persistent drought is most prominent over interior European Russia east of 40°E (VF1) and western Russia, Belarus, and Ukraine (VF3). In support of this result, Borisenkov and Pasetsky (1988, 2003) list several years of drought that occurred in European Russian during this time. Interestingly, this was also a time of a "major long-duration drought" over England and Wales from 1798 to 1808 (Cole and Marsh 2006), and also over north-central Europe as reconstructed by the OWDA (Cook et al. 2015). Connection



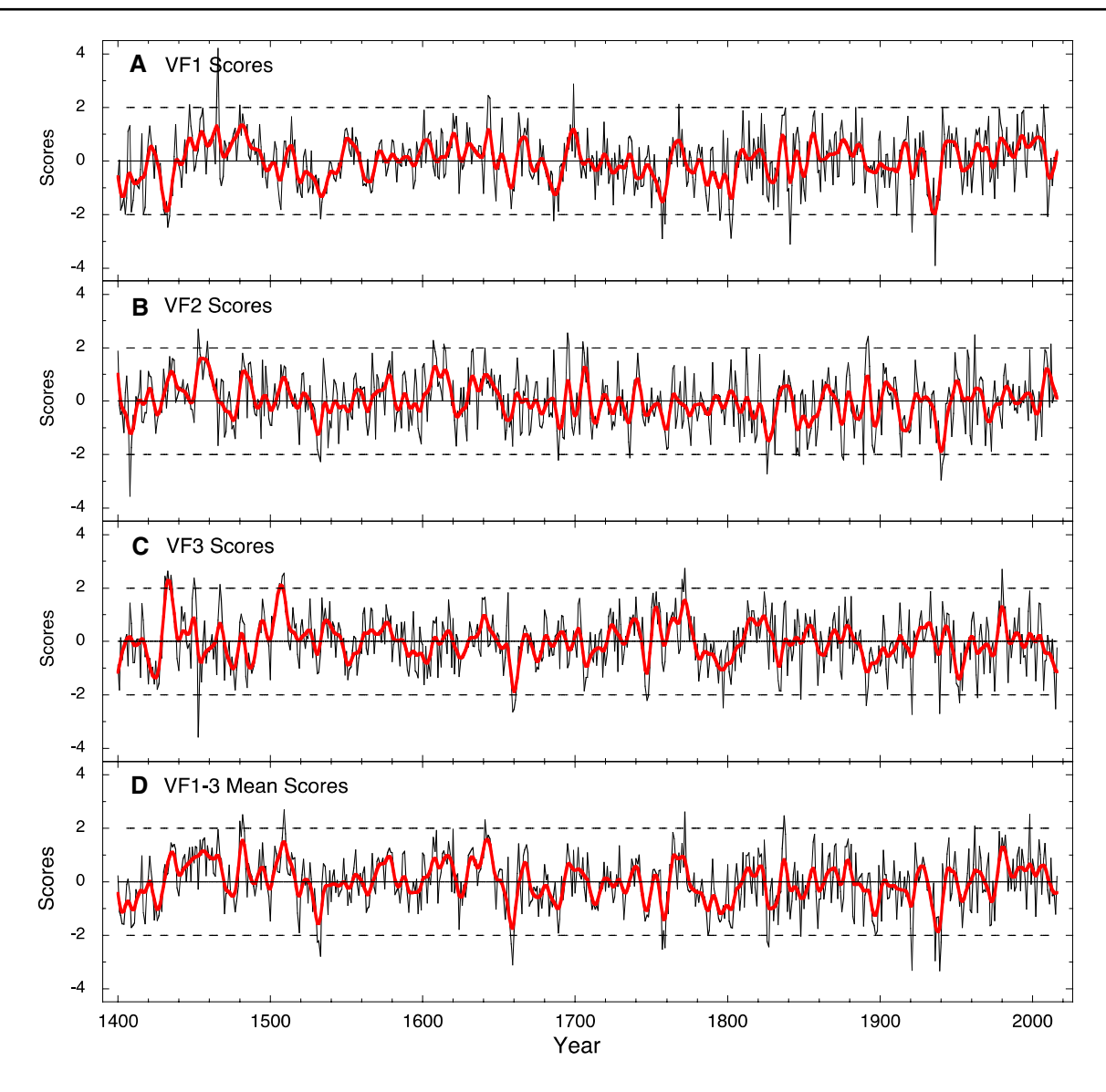


**Fig. 6** Plots of the ERDA Varimax factor scores (VF1-3) corresponding to the factor patterns shown in Fig. 5. In addition, the mean of the three highlights occurrences of pan-ERDA dry and wet years. Each series is shown in units of standard deviation with a 10-year

low-pass filter (red) applied to each. The horizontal dashed lines are the  $\pm 2$  standard deviation limits used for identifying years of extreme drought and wetness

of hydroclimate in the center of European Russia and Eastern Europe was also noted by Matskovsky et al. (2017).

## 7 Comparison to historical droughts

Table 1 highlights in bold red the years for which there are some historical references of droughts at various locations in European Russia (e.g. Borisenkov and Pasetsky 1988, 2003; Kahan 1968). Fewer, but still noteworthy, years of unusual wet conditions are highlighted in bold blue. In each case, the source references for those years are noted. There may be a historical bias in recording the negative impacts

of droughts more frequently than the beneficial impacts of wet events on crop yields, but this is impossible to quantify. Under certain circumstances, wet events can even be as bad as droughts in reducing crop yields (e.g., the 1315–17 "Great Famine" in western Europe; Lucas 1930), but it can be difficult to cleanly separate these impacts in the historical references as well. Also, the quality of the historical data very likely degrades back time from loss of records and changes in reporting locations, thus making definitive comparisons between the ERDA and historical references difficult to judge. Nevertheless, both the VF1 and mean VF1–3 dry extremes have historical references for 12 out of 16 and 11 out 16 dry years, respectively. Thus, there are many more



Table 1 Lists of driest and wettest years in the three Varimax factors estimated from the ERDA (1400–1983), plus the mean of those scores, all scaled in units of standard deviation from the mean

VF1 DRY		VF2 DRY		VF3 DRY		Mean VF1-3 DRY	
Year	<-2SD	Year	<-2SD	Year	<-2SD	Year	<-2SD
1936 <sup>2,3</sup>	-3.897	14081,2	-3.547	1453	-3.560	1939 <sup>2,3</sup>	-3.336
1841 <sup>1</sup>	-3.106	1940	-2.952	1921 <sup>3</sup>	-2.717	1921 <sup>3</sup>	-3.316
1757 <sup>1</sup>	-2.904	$1826^{1}$	-2.721	$1939^{2,3}$	-2.682	1659	-3.109
1802 <sup>1</sup>	-2.888	1941	-2.361	1659	-2.624	$1936^{2,3}$	-2.949
1921 <sup>3</sup>	-2.661	1889 <sup>1,2,3</sup>	-2.356	$1660^{1}$	-2.524	1533 <sup>1,2</sup>	-2.777
1759 <sup>1</sup>	-2.474	1533 <sup>1,2</sup>	-2.258	1797	-2.481	$1757^{1}$	-2.520
1433	-2.355	$1876^{1}$	-2.206	1891 <sup>1,2,3</sup>	-2.394	$1759^{1}$	-2.472
1686	-2.219	1689	-2.201	1952	-2.293	$1827^{1}$	-2.430
1795 <sup>1</sup>	-2.206	1736	-2.117	1747 <sup>1,2</sup>	-2.206	$1658^{1}$	-2.329
1803 <sup>1</sup>	-2.175	1914 <sup>1,2.3</sup>	-2.078	1661	-2.183	1531	-2.266
1533 <sup>1,2</sup>	-2.163	1847 <sup>1</sup>	-2.042	1848 <sup>1,2</sup>	-2.151	1940	-2.258
1434	-2.061	1875 <sup>1,2,3</sup>	-2.031	1964	-2.110	$1826^{1}$	-2.219
1911 <sup>2,3</sup>	-2.040	1942	-2.003	1748 <sup>1,2</sup>	-2.034	1532	-2.213
1417	-2.000	1845	-2.003			1848 <sup>1,2</sup>	-2.039
1431 <sup>1,2</sup>	-1.999	1532	-2.003			1787	-2.002
1934 <sup>2,3</sup>	-1.991					1897 <sup>1,2,3</sup>	-1.999
VF1 WET		VF2 WET		VF3 WET		Mean VF1-3 WET	
Year	>2SD	Year	>2SD	Year	>2SD	Year	>2SD
1466	4.201	1453	2.684	$(1772)^1$	2.731	1509 <sup>1</sup>	2.683
1699 <sup>1</sup>	2.877	$1695^{1,4}$	2.543	1980	2.704	$(1772)^1$	2.602
$(1643)^1$	2.444	1962	2.469	<b>1</b> 433	2.627	1482	2.491
1465	2.419	$(1892)^{1,2,3}$	2.427	$1509^{1}$	2.568	$1837^{1}$	2.470
1644	2.338	$(1607)^1$	2.273	$1435^{1}$	2.477	1641	2.311
1768 <sup>1</sup>	2.113	1459	2.230	$(1431)^{1,2}$	2.437	$1480^{1}$	2.261
$(1447)^1$	2.090	1705	2.225	$(1508)^{1,2}$	2.436	1962	2.085
1480 <sup>1</sup>	2.072	1614 <sup>1</sup>	2.139	$(1450)^1$	2.366		
1941	2.013	$(1891)^{1,2,3}$	2.138	1770 <sup>1</sup>	2.310		
$(1884)^1$	2.001	1696 <sup>1,4</sup>	2.090	1432	2.190		
		$(1708)^1$	2.009	$(1506)^1$	2.162		
		, ,		$(1467)^1$	2.131		
				1507	2.028		

The driest and wettest years are selected as those that equal or exceed  $\pm 2$  standard deviations from the mean. Three years with units exceeding  $\pm 1.99$  standard deviations are also considered close enough to include in these lists. The years in bold red and blue are those years for which there are historical references to dry and wet conditions at various locations in European Russia. These locations are often non-specific, however. Years in parentheses are those that were reconstructed wet, but were historically noted to be dry

Dry year references: <sup>1</sup>Borisenkov and Pasetsky (1988, 2003), <sup>2</sup>Kahan (1968), <sup>3</sup>Schubert et al. (2014)

Wet year references: <sup>1</sup>Borisenkov and Pasetsky (1988, 2003), <sup>4</sup>Neumann and Lindgren (1979)

historical dry "hits" than "misses" overall in the ERDA. The cause for some of these dry "misses" is hard to ascertain. Some may simply be due to inadequate historical data. They could also be associated with unusually cold winter/spring conditions over European Russia (Borisenkov and Pasetsky 1988, 2003; see Table SM1 for examples), which could result in a shorter radial tree growth season and narrower ring width due to unusually cold air temperatures, delayed snow melt, and frozen soil, thus mimicking the narrow rings

more frequently associated with drier conditions. Those suggested years are highlighted in parentheses in the "WET" list in Table 1.

Table B1 in Schubert et al. (2014) also provides a list of droughts and heat waves affecting Eurasia since 1875 based on historical information. We created a composite map from the ERDA of the ten major drought years from that list up to 1930 in Table B1 to avoid biasing the outcome with data from the calibration period. The 10-year composite (lefthand



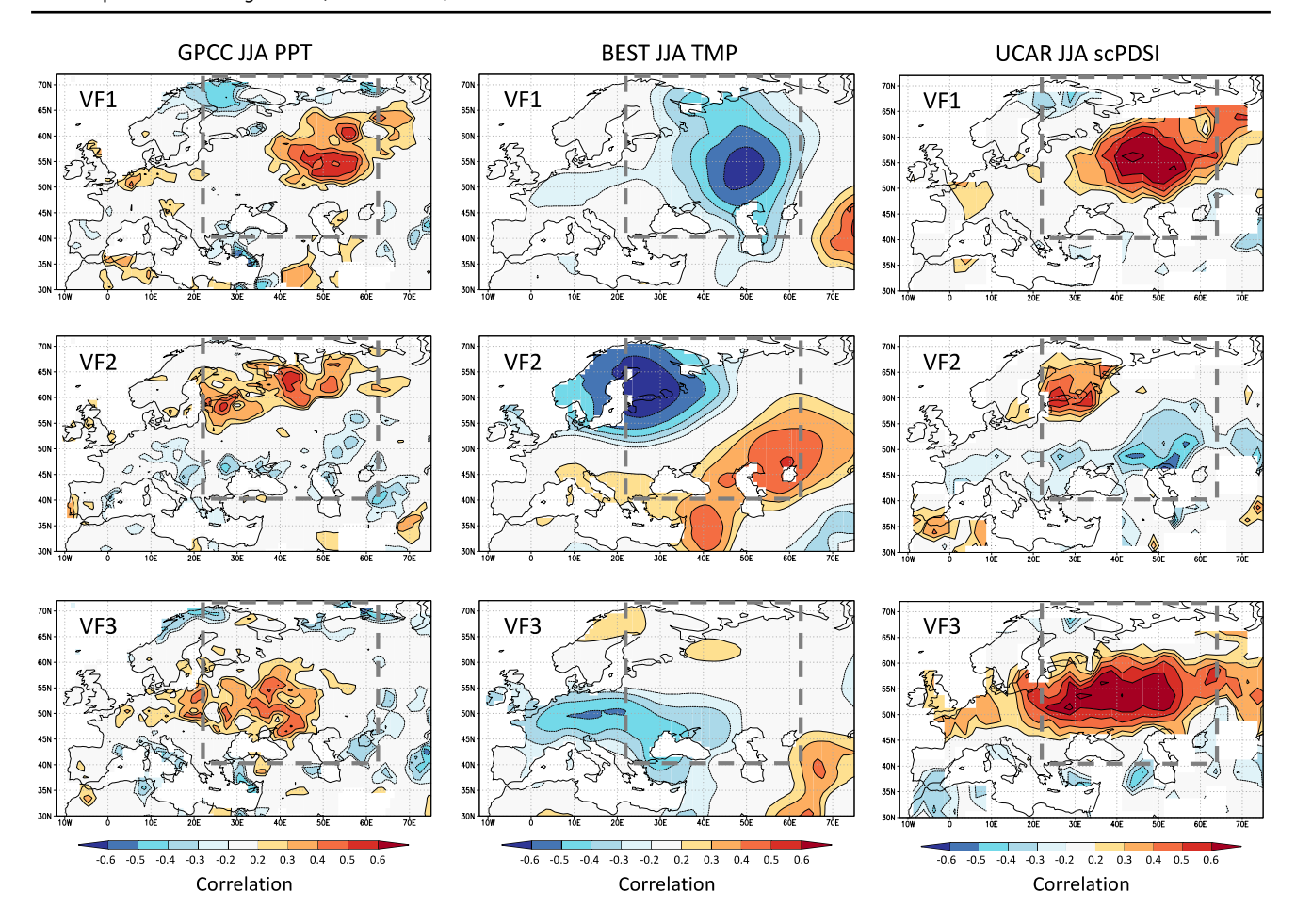


**Fig. 7** Correlations between the Varimax factors (VF1–VF3) and GPCC precipitation, BEST temperature, and UCAR scPDSI data for the same JJA season based on 1891–1983 data. See the text for details on these climate datasets. Correlations > |0.4| are significant at

the 99% confidence level. The rectangle shown in each map delineates the boundaries of the ERDA. The maps are courtesy of KNMI Climate Explorer (van Oldenborgh and Burgers 2005; http://climexp.knmi.nl/)

map) and where its regional mean is statistically significant (righthand map) are shown in Fig. 9, with the specific years used listed in the figure caption. The composite is statistically significant over European Russia south of  $\sim 56^{\circ}$ N, an area that is important to Russian grain production. It is also the area covered mostly by VF3.

## 8 Links to atmospheric circulation

To better understand the likely atmospheric dynamics behind the hydroclimatic patterns expressed by the ERDA Varimax factors, the correlations between their factor scores (Fig. 6) and 700 hPa geopotential heights and 200 hPa meridional winds from the twentieth Century Reanalysis (Compo et al. 2011) are shown in Fig. 10. All calculations were done on the tree-ring only estimates over the 1880–1983 period. The season with the best correlations is May–June–July, beginning 1 month earlier than the June–July–August scPDSI season. This earlier atmospheric dynamics association with

summer drought is similar to that found by Rocheva (2012) in her study of "possible forerunners of droughts", which are linked to the development of persistent anticyclones, drying, and heat waves over Russia (Schubert et al. 2014).

Overall, the locations of the significant negative correlations (blue) with the pressure field are precisely where they should be expected given the locations of the strongly positive (red) factor loadings. Secondary positive correlations (orange) with the pressure field are located southward over the Levant (VF1), southern Volga/Urals (VF2), and northwest Africa (VF3) regions. The circulation pattern associated with VF1, in particular, shows a strong similarity to the circulation anomalies during the mid-summer of 2010. Characterized by anticyclonic circulation over European Russia and low pressure east of the Caspian sea, this is the pattern that drove the concurrent extremes (drought over Russia; floods over Pakistan) that year (Lau and Kim 2012). Additionally, correlations with the 200 hPa meridional winds are quite similar to the correlation patterns between the joint temperature and precipitation rotated principal components



# ERDA Extreme (>|2sd|) Dry and Wet Year Composites

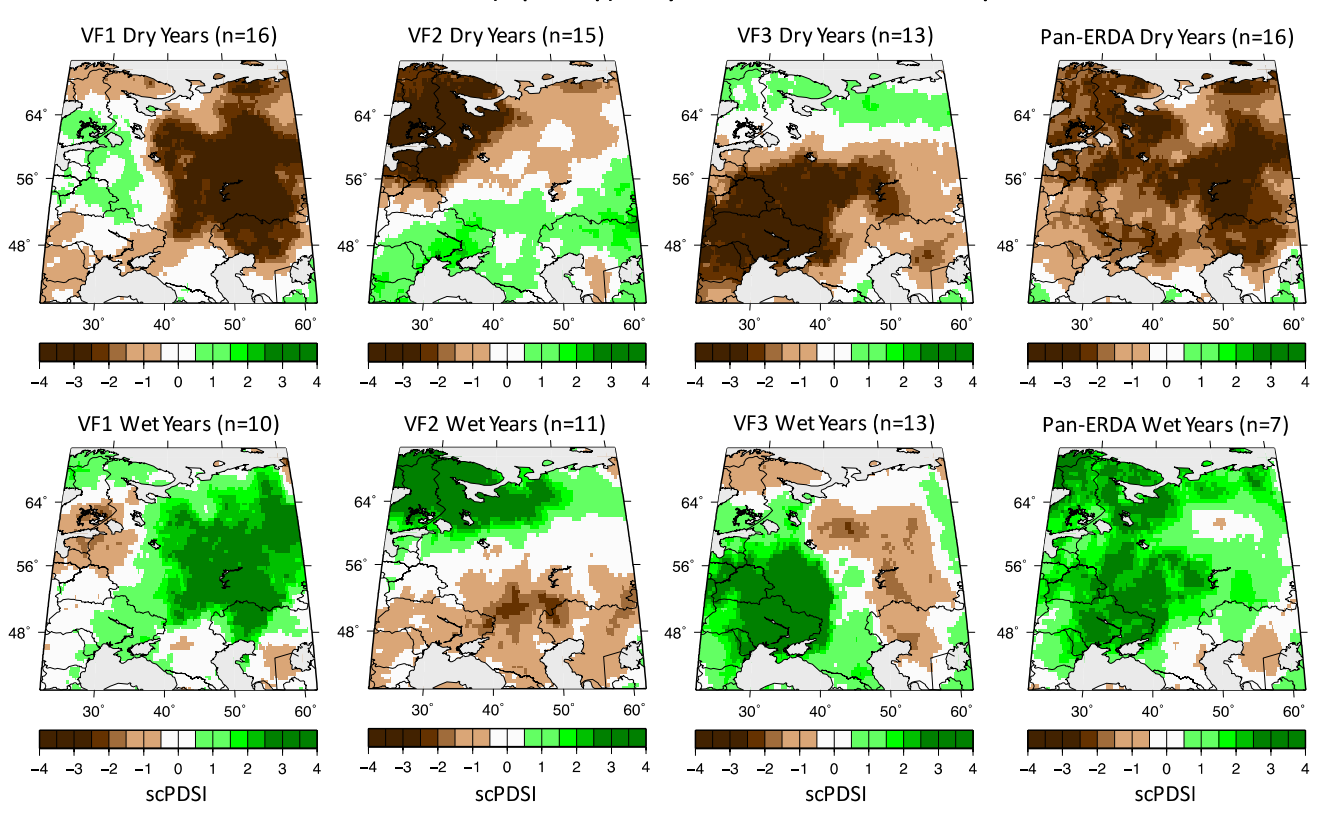


Fig. 8 ERDA extreme ( $>\pm2$ sd) dry and wet year composites with the number of years in each composite indicated. The composites are based on the exceedance years indicated in Fig. 6 and listed in Table 1

Fig. 9 The 10-year composite of years of major historical droughts (lefthand map) extracted from the ERDA, based on the Table B1 list provided by Schubert et al. (2014), and where the regional mean is statistically significant (p < 0.05, two-tailed; righthand map). The drought years composited from the ERDA are 1875, 1891, 1892, 1897, 1901, 1906, 1911, 1920, 1921, and 1924. All selected years purposely predate the calibration period of the ERDA to avoid fitting bias

#### "Schubert" Drought Years >95% C.L. Mean 64° 56° 56 48° 48° 30° 40° 50° 60° 30° 40° 50° 60° 0 -3 0 2 -3 scPDSI scPDSI

(RPCs) and 250 hPa meridional winds in Schubert et al. (2014) (Fig. 6, therein). Correlations with VF1, for example, show strong similarity to the correlation pattern with

RPC1 in Schubert et al. (2014), characterized by anti-phased correlations over Scandinavia and Russia northeast of the Caspian Sea. VF2 from the ERDA is also similar to RPC5



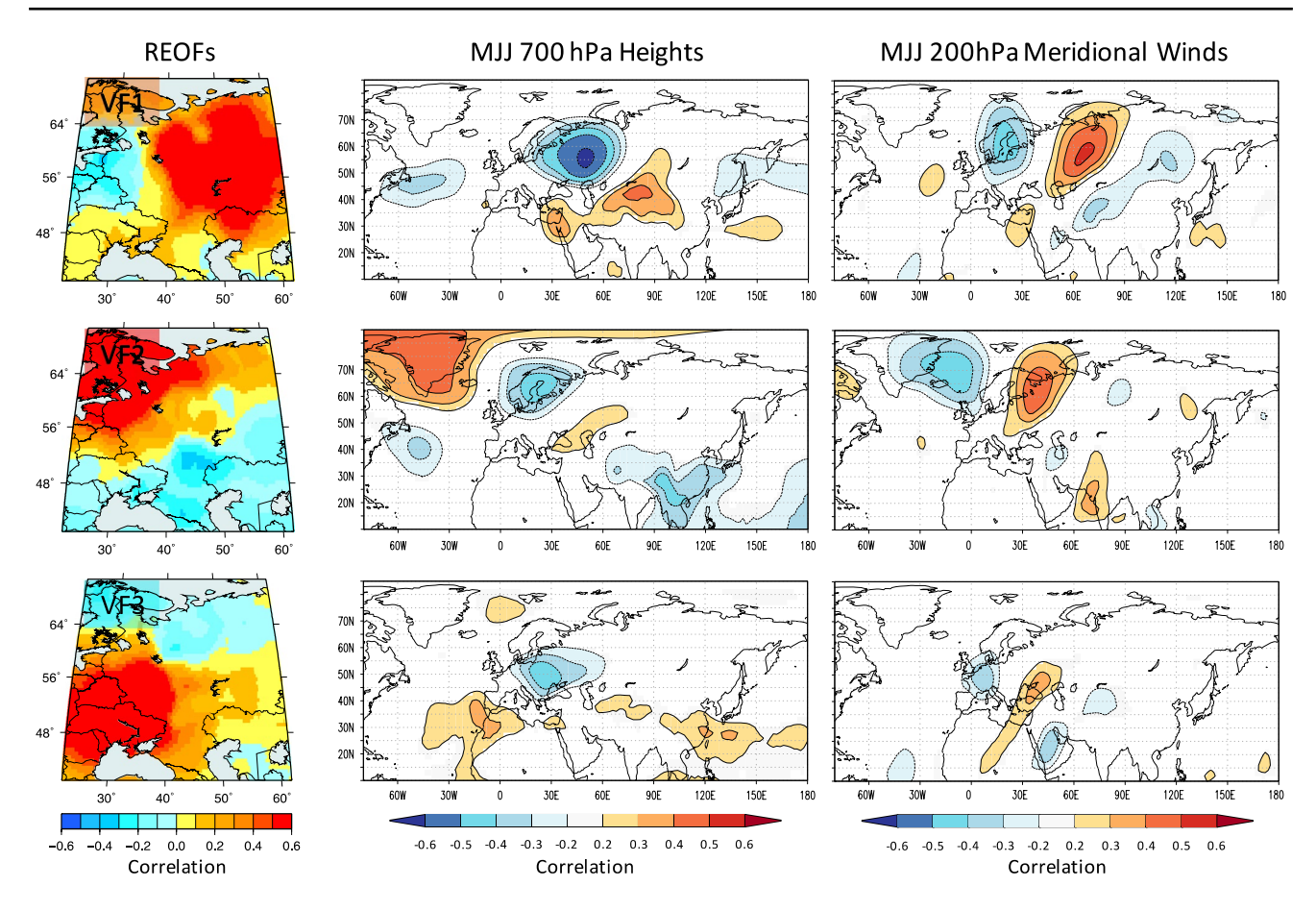


**Fig. 10** Correlations between the ERDA Varimax factors (VF1–3) and May–June–July (MJJ) average 700 hPa heights and 200 hPa meridional winds from the twentieth Century Reanalysis. The analy-

sis period is 1880–1983 and the correlations are based on first-differenced data. The maps are courtesy of KNMI Climate Explorer (van Oldenborgh and Burgers 2005; http://climexp.knmi.nl/)

in Schubert et al. (2014), with major centers of action centered north of Great Britain and over Finland. Along with the previous temperature and precipitation comparisons, these results suggest that the ERDA accurately captures the dominant modes of spatiotemporal climate variability within the region.

## 9 Conclusions

The European Russia Drought Atlas (ERDA) is an important new paleoclimatic reconstruction of drought and wetness that greatly advances our understanding of spatio-temporal hydroclimatic variability over the East European Plain. It is a one-half degree gridded reconstruction of summer scPDSI, covering the period 1400–2016 CE, which was made possible by the development of a critically important new tree-ring network for European Russia and surrounding countries. An ensemble version of the point-by-point regression method (EPPR) was used to reconstruct scPDSI at the grid point level, which makes it compatible with other

paleo-drought atlases based on tree rings, including the proximal Euro-Mediterranean OWDA.

The ERDA has demonstrated skill when compared to instrumental data at the grid point level and compares favorably to recorded instances of historical droughts over European Russia extending back to the fifteenth Century. It is also spatially complete back to 1400 due to the application of a local imputation and smoothing method specifically designed to be compatible with the EPPR reconstruction method. Future papers will investigate the paleoclimate aspects of the ERDA in greater detail in an effort to place modern hydroclimatic variability over European Russia in a long-term context.

REOF analysis has revealed three principal modes of hydroclimate varability in the ERDA that have links to large-scale atmospheric circulation dynamics over northern Eurasia associated with the development of droughts and heat waves there. The planned geographic expansion of this drought atlas to cover all of northern Eurasia is therefore expected to yield a much more complete understanding of hydroclimatic variability and its causes.



**Acknowledgements** Funding for this study was provided to E.R.C. by the Center for Climate and Life at the Lamont-Doherty Earth Observatory of Columbia University. The development of the new tree-ring network in European Russia was spearheaded by O.S. and V.M. through their many contacts with tree-ring scientists in Russia and surrounding countries who generously contributed their tree-ring data for use. The list of co-authors reflects these many contributions. O.S. and V.M. have also received support from the State assignment project no. 0148- 2019-0004 (AAAA-A19-119022190172-5). L.A. received financial support from the State Contract of the Institute of Plant and Animal Ecology, UB RAS (project no. AAAA-A19-119031890086-0) and Russian Fund for Basic Researches (project no. 19-05-00591). E.D. was supported by the Russian Science Foundation project no. 17-77-20123. A.S. was supported by Kungliga Vetenskapsakademien (KVA, including the Margit Althins Stipendiefond), Svenska Sällskapet för Antropologi och Geografi (SSAG), Wilhelm och Martina Lundgrens Vetenskapsfond and Swedish International Development Cooperation Agency SIDA (project SWE-2009-245) and thanks those in Armenia, Kyrgyzstan and Uzbekistan for help in obtaining samples. D.T. was supported by the Russian Foundation for Basic Research and by the Government of the Republic of Tatarstan within the framework of the research project no. 18-44-160028. M.Y. is grateful to the staff of Laboratory of Productivity & Stability of Plant Communities, Institute of Experimental Botany National Academy of Science of Belarus for their help in collection of samples. Belarusian tree-ring chronologies were developed in the project #1.06 "Assessment of the impact of urbanization and land reclamation on the climate, water, land and forest resources of Belarus" of the Belarusian State Research Program "Environmental management and ecology". The ERDA is archived for public availability with the National Centers for Environmental Information, NESDIS, NOAA, U.S. Department of Commerce (http://www. ncdc.noaa.gov/paleo/study/28630). Lamont-Doherty Earth Observatory Contribution No. 8374.

## References

- Agafonov LI, Gurskaya MA (2012) Effect of the longitudinal temperature gradient on the main radial growth of forest trees North—West Siberia. Izvestiya Rossiiskoi Akademii Nauk. Seriya Geograficheskaya 5:48–60 (in Russian)
- Agafonov LI, Gurskaya MA (2013) The influence of the lower ob river runoff on radial growth of trees. Contemp Probl Ecol 6:779–787
- Agafonov LI, Meko D, Panyushkina I (2016) Reconstruction of Ob River, Russia, discharge from ring widths of floodplain trees. J Hydrol 543:198–207
- Alisov BP (1969) Climate of the USSR. Izdatelstvo MGU, Moscow Allen DM (1974) The relationship between variable selection and data augmentation and a method for prediction. Technometrics 16:125–127
- Askeyev OV, Tishin DV, Sparks TH, Askeyev IV (2005) The effect of climate on the phenology, acorn crop and radial increment of pedunculate oak (Quercus robur) in the Middle Volga region, Tatarstan, Russia. Int J Biometeorol 49:262–266
- Babst F, Poulter B, Trouet V, Tan K, Neuwirth B, Wilson R, Carrer M, Grabner M, Tegel W, Levanic T, Panayotov M, Urbinati C, Bouriaud O, Ciais P, Frank D (2013) Site- and species-specific responses of forest growth to climate across the European continent. Glob Ecol Biogeogr 22:706–717
- Barnston AG, Livezey RE (1987) Classification, seasonality, and persistence of low-frequency atmospheric circulation patterns. Mon Weather Rev 115:1083–1126
- Berk KN (1984) Validating regression procedures with new data. Technometrics 26(4):331–338

- Bhalme HN, Mooley DA (1980) Large-scale droughts/floods and monsoon circulation. Mon Weather Rev 108:1197–1211
- Bogolepov MA (1907) About climatic fluctuations of European Russia during historical time. Earth Sci (Zemlevedeniye) 3:1–188 (in Russian)
- Bogolepov VA (1922) Causes of poor harvest and starvation in Russia in the historical period. Novaya Derevnya, Moscow (in Russian)
- Borisenkov EP, Pasetsky VM (1988) Thousand-year chronicle of unusual phenomena of nature. Mysl, Moscow (in Russian)
- Borisenkov EP, Pasetsky VM (2003) Chronicle of unusual natural event during the last 2.5 millennia. Gidrometizdat, St. Petersburg (in Russian)
- Briffa KR, Jones PD, Schweingruber FH, Shiyatov SG, Cook ER (1995) Unusual twentieth-century summer warmth in a 1000-year temperature record from Siberia. Nature 376:156–159
- Buchinsky IE (1957) On the past climate of the Russian Plain. Gidrometizdat, Leningrad (in Russian)
- Buchinsky IE (1976) Droughts and dry winds. Gidrometeoizdat, Leningrad (in Russian)
- Cattell RB (1966) The scree test for the number of factors. Multivar Behav Res 1(2):245–276
- Cherenkova EA (2007) Dynamics of severe atmospheric droughts in European Russia. Russ Meteorol Hydrol 32(11):675–682
- Chernavskaya M (1995) Intrasecular air temperature changes in the North European Russia over the last millennium. International Conference on Past, Present and Future Climate. 22–25 August. Helsinki, Finland, pp 119–121
- Cole GA, Marsh TJ (2006) The impact of climate change on severe droughts. Major droughts in England and Wales from 1800 and evidence of impact, in Science Report:SC040068/SR1 (Environment Agency, Bristol, UK, 2006)
- Compo GP, Whitaker JS, Sardeshmukh PD, Matsui N, Allan RJ, Yin X, Gleason BE, Vose RS, Rutledge G, Bessemoulin P, Brönnimann S, Brunet M, Crouthamel RI, Grant AN, Groisman PY, Jones PD, Kruk M, Kruger AC, Marshall GJ, Maugeri M, Mok HY, Nordli Ø, Ross TF, TrigoRM Wang XL, Woodruff SD, Worley SJ (2011) The twentieth century reanalysis project. Q J R Meteor Soc 137:1–28
- Cook ER, Peters K (1997) Calculating unbiased tree-ring indices for the study of climatic and environmental change. Holocene 7(3):359–368
- Cook ER, Briffa KR, Jones PD (1994) Spatial regression methods indendroclimatology: a review and comparison of two techniques. Int J Climatol 14:379–402
- Cook ER, Briffa KR, Meko DM, Graybill DA, Funkhouser G (1995) The segment length curse in long tree-ring chronology development for paleoclimatic studies. Holocene 5(2):229–237
- Cook ER, Meko DM, Stahle DW, Cleaveland MK (1999) Droughtreconstructions for the continental United States. J Clim 12:1145–1162
- Cook ER, Woodhouse C, Eakin CM, Meko DM, Stahle DW (2004) Long-term aridity changes in the western United States. Science 306:1015–1018
- Cook ER, Krusic PJ, Anchukaitis KJ, Buckley BM, Nakatsuka T, Sano M, Asia2k Members (2013) Tree-ring reconstructed summer temperature anomalies for temperate East Asia since 800 C.E. Clim Dyn 41:2957–2972. https://doi.org/10.1007/s0038 2-012-1611-x
- Cook ER, Seager R, Kushnir J, Briffa KR, Buentgen U, Frank D, Krusic PJ, Tegel W, van der Schrier G, Andreu-Hayles L, Baillie M, Baitttinger C, Bleicher N, Bonde N, Brown D, Carrer M, Cooper R, Cufar K, Dittmar C, Esper J, Griggs C, Gunnarson B, Gunther B, Gutierrez E, Haneca K, Helema S, Herzig F, Heussner K-U, Hofmann J, Janda J, Kontic R, Kose N, Kyncl T, Levanic T, Linderholm H, Manning S, Melvin T, Miles D, Neuwirth B, Nicolussi K, Nola P, Panayotov M, Popa I, Rothe A, Seftigen K,



- Seim A, Svarva H, Svoboda M, Thun T, Timonen M, Touchan R, Trotsiuk V, Trouet V, Walder F, Wazny T, Wilson R, Zang C (2015) Old world megadroughts and pluvials during the Common Era. Sci Adv 1(10):e1500561. https://doi.org/10.1126/sciadv.1500561
- Dai A, Zhao T (2017) Uncertainties in historical changes and future projections of drought. Part I: estimates of historical drought changes. Clim Change 144(3):519–533. https://doi.org/10.1007/ s10584-016-1705-2
- Dolgova EA (2016) June–September temperature reconstruction in the Northern Caucasus based on blue intensity data. Dendrochronologia 39:17–23
- Dronin NM, Bellinger EG (2005) Climate dependence and food problems in Russia, 1900–1990: the interaction of climate and agricultural policy and their effect on food problems. Central European University Press, Budapest
- Drozdov OA (1980) Droughts and humidity dynamics. Gidrometeoizdat, Leningrad (In Russian)
- Esper J, Shiyatov S, Mazepa V, Wilson R, Graybill D, Funkhouser G (2003) Temperature-sensitive Tien Shan tree ring chronologies show multi-centennial growth trends. Clim Dyn 21:699–706
- Fritts HC (1976) Tree rings and climate. Academic Press, New York Gazina EA, Klimenko VV (2008) Climatic changes of the Eastern Europe during the last 250 years by instrumental data. Moscow University Bulletin. Series 5. Geography 3:60–66
- Gershunov A, Douville H (2008) Extensive summer hot andcold extremes under current and possible future climaticconditions: Europe and North America. In: Diaz HF, Murnane RJ (eds) Climate extremes and society. Cambridge University Press, Cambridge, pp 74–98
- Golubev G, Dronin N (2004) Geography of droughts and food problems in Russia (1900–2000), Report No. A 0401. (Center for Environmental Systems Research, University of Kassel, Kurt-Wolters-Str. 3, 34109 Kassel, Germany. (http://www.usf.unikassel.de)
- Graybill D, Shiyatov S, Burmistrov V (1992) Recent dendrochronological investigations in Kirghizia, USSR. Lundqua Rep 34:123–127
- Gurskaya M, Hallinger M, Singh J, Agafonov L, Wilmking M (2012)
  Temperature reconstruction in the Ob River valley based on ring widths of three coniferous tree species. Dendrochronologia 30(4):302–309
- Guttman L (1954) Some necessary conditions for common-factor analysis. Psychometrika 19:149–161
- Helama S, Lindholm M (2003) Droughts and rainfall in south eastern Finland since AD 874, inferred from Scots pine tree-rings. Boreal Environ Res 8:171–183
- Hellmann L, Agafonov L, Charpentier Ljungqvist F, Churakova O, Düthorn E, Esper J, Hülsmann L, Kirdyanov AV, Moiseev P, Myglan VS, Nikolaev AN, Reinig F, Schweingruber FH, Solomina O, Tegel W, Büntgen U (2016) Diverse growth trends and climate responses across Eurasia's boreal forest. Environ Res Lett. https://doi.org/10.1088/1748-9326/11/7/074021
- Kahan A (1968) Natural calamities and their effect upon the food supply of Russia. Jahrbücherfür Geschichte Osteuropas (Yearbooks for the history of Eastern Europe) 16(3):353–377
- Kaiser HF (1958) The Varimax criterion for analytic rotation in factor analysis. Psychometrika 23:187–200
- Kaiser HF (1960) The application of electronic computers to factor analysis. Educ Psychol Meas 20:141–151
- Karl TR, Koscielny AJ (1982) Drought in the United States. J Clim 2:313–329
- Karpukhin AA, Matskovsky VV (2014) Absolute generalized treering chronology of Sheksna and Sukhona rivers catchments (AD 1085–2009). Russ Archaeol 2:76–87 (in Russian)
- Kiselev S, Romashkin R, Nelson GC, Mason-D'Croz D, Palazzo A (2013) Russia's food security and climate change: looking

- into the future. Economics: the open-access. Open-Assess E-J 7:2013-2039
- Kleschenko AD (2005) Monitoring agricultural drought in Russia. In: Boken V, Cracknell AP, Heathcote RL (eds) Monitoring and predicting agricultural drought. Oxford University Press, Oxford, pp 196–207
- Klimenko V, Solomina ON (2010) Climatic variations in the East European plain during the last millennium: state of the art. In: Przybylak R et al (eds) The polish climate in the European context: an historical overview. Springer, Berlin, pp 71–102. https://doi.org/10.1007/978-90-481-3167-9\_3
- Knysh NV, Yermokhin MV (2019) The effects of climatic factors in forming increment of English oak (*Quercus robur* L.) in south regions of Belarus. Proc Natl Acad Sci Belarus Biol Ser 64(2):169–179 (in Russian)
- Kolchin BA (1963) Dendrochronology of Novgorod. Materials and research of archaeology of USSR. AN SSSR, Moscow (in Russian)
- Krenke AN, Chernavskaya MM (1998) Spatial and temporal variations of the frequency of extreme climatic events in the Russian Plain. Izvestiya Rossiiskoi Akademii Nauk. Seriya Geograficheskaya 5:53–61
- Kulakova M (2009) A dendrochronological analysis of wood from Pskov. Archaeol Ethnol Anthropol Eurasia 37(1):71–76
- Kupfer AY (1846) Conclusions from meteorological records performed in the Russian State and stored in the meteorological archive of Academy of Sciences. Academy of Sciences, St. Petersburg
- Kutzbach JE (1967) Empirical eigenvectors of sea-level pressure, surface temperature and precipitation complexes over North America. J Appl Meteorol 6:791–802
- LaMarche VC Jr, Fritts HC (1971) Anomaly patterns of climate over the western United States, 1700–1930, derived from principal component analysis of tree-ring data. Mon Weather Rev 99:139–142
- Lau WK, Kim KM (2012) The 2010 Pakistan flood and Russian heat wave: teleconnection of hydrometeorological extremes. J Hydrometeor 13(1):392–403
- Lorenz EN (1956) Empirical orthogonal functions and statistical weather prediction. Statistical Forecasting Project Report 1, MIT Department of Meteorology, p 49
- Lucas HS (1930) The great European famine of 1315, 1316, and 1317. Speculum 5(4):343–377
- Matskovsky V (2016) Climatic signal in tree-ring width chronologies of conifers in European Russia. Int J Climatol 36:3398–3406
- Matskovsky V, Dolgova E, Lomakin N, Matveev S (2017) Dendroclimatology and historical climatology of Voronezh region, European Russia, since 1790s. Int J Climatol 37:3057–3066
- Matveev SM, Tarankov VI, Shurygin YN (2012a) Dendroclimatological analysis of the natural forest and forest plantations of scots pine (*Pinus sylvestris* L.) in dry-moist site conditions of the Khrenovoe pine forest. Nauchn zh Kuban gosagraruniv 75(1):1–12 (in Russian)
- Matveev SM, Matveeva SV, Shurygin YN (2012b) Recurrence of severe droughts and long-term dynamics of radial increment of the scots pine in the Usman and Khrenovoe forests in the Voronezh region. J Sib Federal Univ Biol 5(1):27–42 (in Russian)
- Melvin TM, Briffa KR (2008) A "signal-free" approach to dendroclimaticstandardisation. Dendrochronologia 26:71–86
- Melvin TM, Briffa KR, Nicolussi K, Grabner M (2007) Time-varyingresponse smoothing. Dendrochronologia 25:65–69
- Meshcherskaya AV, Blazhevich VG (1997) The drought and excessive moisture indices in a historical perspective in the principal grain-producing regions of the former Soviet Union. J Clim 10:2670–2682
- Mitchell JM, Stockton CW, Meko DM (1979) Evidence of a 22-year rhythm of drought in the western United States related to the



- Hale solar cycle since the seventeenth century. In: McCormac BM, Seliga TA (eds) Solar-terrestrial influences on weather and climate. D. Reidal, Dordrecht, pp 125–144
- Muller RA, Curry J, Groom D, Jacobsen R, Perlmutter S, Rohde R, Rosenfeld A, Wickham C, Wurtele J (2013) Decadal variations in the global atmospheric land temperatures. J Geophys Res-Atmos. https://doi.org/10.1002/jgrd.50458
- Neumann J, Lindgrén S (1979) Great historical events that were significantly affected by the weather: 4, The great famines in Finland and Estonia, 1695–97. Bull Am Meteorol Soc 60(7):775–787
- North GR, Bell TL, Cahalan RF, Moeng FJ (1982) Sampling errors in the estimation of empirical orthogonal functions. Mon Weather Rev 110:699–706
- Obukhov AM, Kurganskii MV, Tatarskaya MS (1984) Dynamical conditions of drought and other large-scale weatheranomalies formation. Sov Meteorol Hydrol 10:5–13 (in Russian)
- Osborn TJ, Barichivich J, Harris I, van der Schrier G, Jones PD (2017) Monitoring global drought using the self-calibrating Palmer drought severity index [in "State of the Climate in 2016"]. B Am Meteorol Soc 98:S32–S33
- Pavlova V, Shkolnik I, Pikaleva A, Efimov S, Karachenkova A, Kattsov V (2019) Future changes in spring wheat yield in the European Russia as inferred from a large ensemble of high-resolution climate projections. Environ Res Lett 14:034010
- Picard RR, Berk KN (1990) Data splitting. Am Stat 44:140-147
- Potop V, Soukup J (2009) Spatiotemporal characteristics of dryness and drought in the Republic of Moldova. Theor Appl Climatol 96(3):305–318
- Preisendorfer RW, Zwiers FW, Barnett TP (1981) Foundations of principal component selection rules. SIO Reference Series 81-4, Scripps Institution of Oceanography, p 192
- Quan NT (1988) The prediction sum of squares as a general measure for regression diagnostics. J Bus Econ Stat 6:501–504
- Rauner YuL (1981) Dynamics of humidity extremes in historical period. Izvestiya Rossiiskoi Akademii Nauk. Seriya Geograficheskaya 6:5–22 (in Russian)
- Richman MB (1986) Rotation of principal components. J Clim 6:293-335
- Rocheva EV (2012) Possible forerunners of droughts in agricultural areas of Russia. Russ Meteorol Hydrol 37:575–585
- Rudenko AI (ed) (1958) Droughts in the USSR. Their origin, frequency of occurrence and impact on yield. Gidrometeoizdat, Leningrad (in Russian)
- Schneider U, Becker A, Finger P, Meyer-Christoffer A, Ziese M (2018) GPCC full data monthly product version 2018 at 1.0°: monthly land-surface precipitation from rain-gauges built on GTS-based and historical data. Res Data Arch. https://doi.org/10.5676/dwd\_gpcc/fd\_m\_v2018\_100
- Schubert SD, Wang H, Suarez M (2011) Warm season subseasonal variability and climate extremes in the Northern Hemisphere: the role of stationary Rossby waves. J Clim 24:4773–4792. https://doi.org/10.1175/JCLI-D-10-05035.1
- Schubert SD, Want H, Koster RD, Suarez MJ, Groisman PY (2014) Northern Eurasian heat waves and droughts. J Clim 27:3169-3207
- Schubert SD, Stewart RE, Wang H, Barlow M, Berbery EH, Cai W, Hoerling M, Kanikicharla K, Koster R, Lyon B, Mariotti A, Mechosa CR, Müller O, Rodriguez-Fonseca B, Seager R, Seneviratne SI, Zhang L, Zhou T (2016) Global meteorological drought: a synthesis of current understanding with a focus on SST drivers of precipitation deficits. J Clim 29(11):3989–4019
- Seftigen K, Björklund J, Cook ER, Linderholm HW (2015) A tree-ring field reconstruction of Fennoscandian summer hydroclimate variability for the last millennium. Clim Dyn 44:3141–3154

- Seftigen K, Goosse H, Klein F, Chen D (2017) Hydroclimate variability in Scandinavia over the last millennium—insights from a climate model-proxy data comparison. Clim Past 13:1831–1850
- Seim A, Omurova G, Azisov E, Musuraliev K, Aliev K, Tulyaganov T, Nikolyai L, Botman E, Helle G, Liñan ID, Jivcov S, Linderholm HW (2016a) Climate change increases drought stress of juniper trees in the mountains of Central Asia. PLoS One 11(4):e0153888. https://doi.org/10.1371/journal.pone.0153888
- Seim A, Tulyaganov T, Omurova G, Nikolyai L, Botman E, Linderholm HW (2016b) Dendroclimatological potential of three juniper species from the Turkestan range, northwestern Pamir-Alay Mountains, Uzbekistan. Trees 30:733–748
- Shostakovich VB (1934) Silt lake deposits and periodic variations of natural events. Zapiski Gosudarstvyenogo Gidrologicheskogo Instituta 13:94–108
- Shvedov FN (1892) Tree as a chronicle of droughts. Meteorol Bull 5:37–49
- Solomina O, Davi N, D'Arrigo R, Jacoby G (2005) Tree-ring reconstruction of Crimean drought and lake chronology correction. Geophys Res Lett 32:L19704. https://doi.org/10.1029/2005G L023335
- Solomina ON, Matskovsky VV, Zhukov RS (2011) The Vologda and Solovki dendrochronological "chronicles" as a source of information about the climate conditions of the last millennium. Dokl Earth Sci 439:1104–1109. https://doi.org/10.1134/S1028334X1 1080071
- Solomina ON, Dolgova EA, Maximova OE (2012) Tree-ring based hydrometeorological reconstructions in Crimea, Caucasus and Tien-Shan. Nestor Istoriya, St. Petersburg
- Solomina O, Maximova O, Cook E (2014) Picea schrenkiana ring width and density at the upper and lower tree limits in the Tien Shan mts Kyrgyz republic as a source of paleoclimatic information. Geogr Environ Sustain 1(7):66–79
- Solomina ON et al (2017) Droughts of the East European Plain according to hydrometeorological and tree-ring data. Nestor Istoriya, St. Petersburg
- St George S, Ault TR (2014) The imprint of climate within Northern Hemisphere trees. Quat Sci Rev 89:1–4
- Stefanon M, D'Andrea F, Drobinski P (2012) Heatwaveclassification over Europe and the Mediterranean region. Environ Res Lett 7:014023. https://doi.org/10.1088/1748-9326/7/1/014023
- Tarabardina OA (2009) Environmentand human behavior in northern dendrochronological studies of medieval Novgorod Novgorod (based on the findings of archaeological excavations 1991–2006). Archaeol Ethnol Anthropol Eurasia 37(1):77–84
- Tishin DV, Chizhikova NA, Chugunov RG (2014) Radial growth of pine (*Pinus sylvestris* L.) swamps as an indicator of local climate change. For Bull 5:177–182 (in Russian)
- Trouet V, van Oldenborgh GJ (2013) KNMI climate explorer: a webbased research tool for high-resolution palaeoclimatology. Tree-Ring Res 69:3–13
- van der Schrier G, Barichivich J, Briffa KR, Jones PD (2013) A scP-DSI-based global data set of dry and wet spells for 1901–2009. J Geophys Res-Atmos 118:4025–4048
- van Oldenborgh GJ, Burgers G (2005) Searching for decadal variations in ENSO precipitation teleconnections. Geophys Res Lett 32(15):L15701. https://doi.org/10.1029/2005GL023110
- Veselovsky KS (1857) On the climate of Russia. Imperial Academy Press, St. Petersburg (in Russian)
- Vil'd GI (1882) New normal and five years mean air temperature. Imperial Academy Press, St. Petersburg (in Russian)
- Volkov IM (1992) The drought and famine of 1946–47. Russ Stud Hist 31(2):31–60
- Voronov AM (1992) Estimate of the regional changes of hydroclimatic conditions at the European part of Soviet Union according to historical data. Water Res 4:97–105 (in Russian)



Wahlén E (1886) True daily means and daily variation of temperature at 18 stations of the Russian Empire. Meteorol Sb 3:586

Wells N, Goddard S, Hayes MJ (2004) A self-calibrating palmer drought severity index. J Clim 17:2335–2351

Yermokhin MV, Knysh NV (2016) Climate and grazing impact on a radial increment of oak (*Quercus robur* L.). Nat Resour 2:67–74 (in Russian)

**Publisher's Note** Springer Nature remains neutral with regard to jurisdictional claims in published maps and institutional affiliations.

